Journal of Metals, Materials and Minerals, Vol. 31, No. 3, pp. 20-26, 2021

Investigations on phase coexistence and functional properties of BCZT lead-free piezoceramic

Jirapa TANGSRITRAKUL[1,*], Thiyanee SONKAMI[1], Chumpon WICHITTANAKOM[2], Chotiros DOKKHAN[3], and Panithi WIROONPOCHIT[3]

[1] *Department of Materials and Textile Technology, Faculty of Science and Technology, Thammasat University, Pathum Thani, 12120, Thailand*
[2] *Department of Physics, Faculty of Science and Technology, Thammasat University, Pathum Thani, 12120, Thailand*
[3] *National Metal and Materials Technology Center, Thailand Science Park, Pathum Thani 12120, Thailand*

***Corresponding author e-mail:** tjirapa@tu.ac.th

Received date:
26 August 2020
Revised date
30 May 2021
Accepted date:
31 May 2021

Keywords:
Lead-free piezoceramics;
Phase coexistence;
Rietveld refinement;
Ferroelectric properties;
Barium Titanate

Abstract

Large piezoelectric properties was observed in (1-x)BZT-(x)BCT where x=0.5 or $Ba_{0.85}Ca_{0.15}Ti_{0.9}Zr_{0.1}O_3$ (denoted as BCZT), leading to a promising candidate for lead-free piezoelectric materials. However, phase formation of the BCZT is controversial and still unclear since various phase coexistences were identified in the literatures, for instances, the mixed phases of rhombohedral-tetragonal (R-T), ortho-rhombic-tetragonal (O-T) or rhombohedral-orthorhombic-tetragonal (R-O-T). Additionally, it is well known that the crystal structure plays a crucial role on the occurrence of polarization in the piezoceramics. Therefore, this work aims to investigate the coexistence of phase formation at room temperature for the BCZT powder and ceramic. Moreover, the electrical properties as a function of temperature, frequency and electric field were observed in order to evaluate the extrinsic contribution of piezoelectric response. It was found that, according to the results from temperature-dependent dielectric properties as well as Rietveld refinement of XRD profiles, the coexistence of O-T phase was observed in the BCZT powder and ceramic. Furthermore, the enhancement of Ca^{2+} substitution into Ba^{2+} site in BCZT ceramic caused the shrinkage of unit cell, leading to the shift of XRD profile and Raman spectra. In addition, it was found that the applications of frequency and electric field can influence on changes of domain-wall motion and micro-polar cluster in the BCZT piezoceramic.

1. Introduction

Barium Titanate ($BaTiO_3$ or BT) is the first polycrystalline ceramic that discovered ferroelectric properties during World War II. Thus, it was mainly used as capacitors due to its high dielectric permittivity (ε_r) [1]. Later, in 1950s, Lead Zirconate Titanate ($PbZr_{1-x}Ti_xO_3$ or PZT) was founded outstanding dielectric, ferroelectric and piezoelectric properties with high Curie temperature (T_C), especially at the morphotropic phase boundary (MPB) composition that observed rhombohedral-tetragonal (R-T) phase coexistence. Therefore, PZT has been widely used in various applications such as thin-film capacitors, piezoelectric sensors, transducers, actuators, etc.

However, PZT contains a toxic Pb that become a major concern for health and environmental issues. Hence, European Union (EU) has launched the legislations to restrict hazardous substance including Pb [2]. As a result, new candidates of lead-free piezoelectric ceramics have been explored, for instance, Barium Titanate-based, Potassium Sodium Niobate-based or Bismuth-based piezoceramics [3,4]. In 2009, the large piezoelectric coefficient (d_{33}) of 620 pC/N was observed at room temperature in lead-free piezoelectric system of (1-x) $BaTi_{0.8}Zr_{0.2}O_3$-(x)$Ba_{0.7}Ca_{0.3}TiO_3$ where x=0.5 or $Ba_{0.85}Ca_{0.15}Zr_{0.1}Ti_{0.9}O_3$ which attributed to the occurrence of rhombohedral-tetragonal (R-T) mixed phases at MPB, similar to MPB for PZT system, as reported by Liu *et al.* [5]. This observation shows that the (1-x)BZT-(x)BCT piezoceramic is a promising candidate for PZT replacement [6].

Although Liu suggested phase diagram of (1-x)BZT-(x)BCT piezo-ceramic with R-T coexist phases at MPB composition (x~0.5), Keeble later found the occurrence of orthorhombic phase in (1-x) BZT-(x)BCT piezoceramic at MPB composition, leading to the modification of (1-x)BZT-(x)BCT phase diagram [7]. Consequently, while many publications reported that the phase formation of (1-x) BZT-(x)BCT where x=0.5 was R-T mixed phases as indicated in the previous phase diagram [5,8-10], the coexistence of orthorhombic- tetragonal (O-T), monoclinic-tetragonal (M-T), or rhombohedral-orthorhombic-tetragonal (R-O-T) also found by others [11-13]. Moreover, some researchers have mentioned that it is difficult to identify phase formation of (1-x)BZT-(x)BCT where x=0.5 [14-15]. This signifies that the identification of phase formation for (1-x) BZT-(x)BCT where x=0.5 or $Ba_{0.85}Ca_{0.15}Ti_{0.9}Zr_{0.1}O_3$ is still unclear and controversial.

It is well known that the intrinsic contribution of piezoelectric response for piezoelectric materials is attributed to lattice distortion and polarization which originated from the crystal structure [16]. Furthermore, the phase coexistence can also increase the polarization direction, leading to the enhancement of electrical properties [14].

Therefore, the aims of this work is to identify the coexisting phases at room temperature for the (1-x)BZT-(x)BCT where x=0.5 or $Ba_{0.85}Ca_{0.15}Ti_{0.9}Zr_{0.1}O_3$ powder and ceramic which prepared by the conventional mixed-oxide method. In addition, further investigations on the dielectric and ferroelectric properties were investigated in order to understand the impact of phase coexistence on the functional properties.

2. Experimental

$Ba_{0.85}Ca_{0.15}Ti_{0.9}Zr_{0.1}O_3$ (referred as BCZT) powder was prepared by mixed-oxide method using $BaCO_3$ (99.0%), $CaCO_3$ (99.0%), TiO_2 (99.0%), and ZrO_2 (99.0%) as the starting materials. The raw powders were weighed according to the composition and milled in ethanol (99.5%) for 24 h using yttria-stabilised zirconia (YSZ) media with diameter of 5 mm. Then, the slurry was dried in an oven at 90°C for 24 h, prior to calcination at 1250°C for 3 h using heating/cooling rates of 5°C·min^{-1} in order to obtain the BCZT powder. For ceramic preparation, the calcined powder was ground and mixed with 3 wt% of polyvinyl alcohol (PVA) as a binder by agate mortar and pestle before pressing under a uniaxial pressure of 200 MPa into a disc shape with diameter of 8 mm and thickness of 1.5 mm. Next, the green pellets were sintered at 1400°C for 3 h with heating/cooling rates of 5°C·min^{-1} in order to obtain the BCZT ceramic.

For material characterizations, the density of sintered ceramic was measured by Archimedes method. The scanning electron microscope (JEOL, JCM-6000) was employed to observe the particle morphology of the calcined powder and the microstructure the sintered ceramic. The XRD profiles of BCZT powder and ceramic were obtained using an X-ray diffractometer (Bruker, D8 ADVANCE). Room-temperature Raman spectra were observed with Fourier Transform Raman Spectrometer (Nicolet iS50, Thermo Scientific, USA). The identification of phase formation was done by Rietveld refinement using GSAS-II software for both BCZT powder and ceramic [17]. For electrical measurements, the parallel surfaces of ceramic pellets were ground using SiC papers from grade P400, P600, and P800, respectively. Then, the silver electrodes were applied on the ground surface of the BCZT ceramic prior to measuring the electrical properties. The LCR meter (Agilent E4980A precision) was employed to determine the relative permittivity and loss tangent as a function of temperature (between 30°C and 200°C as well as frequency (between 10 Hz and 1 MHz). The ferroelectric P-E hysteresis loops were measured at room temperature as a function of electric field (between 5 kV·cm^{-1} and 40 kV·cm^{-1}) by Radiant ferroelectric test system (Precision Premier II, Albuquerque, New Mexico).

3. Results and discussions

3.1 SEM observation

The SEM micrograph of BCZT powder calcined at 1250°C for 3 h is shown in Figure 1(a). It was found that the average particle size of the grinding powder was less than 1 μm, while the average grain size of sintered ceramic was around 7.41 μm. Figure 1(b) shows the surface microstructure of BCZT ceramic sintered at 1400°C for 3 h which established bulk density of 5.50 g·cm^{-3} (96.4% of the theoretical density) [18]. The abnormal grain growth with polyhedron shape was observed in the BCZT ceramic, similar to the BCZT ceramic that prepared using hydrothermal method. [19] Moreover, the terraced surface and intergranular pore were found, as indicated by the arrows in Figure 1(b). This terraced surface was also observed in the BCZT ceramic prepared by modified Pechini and hydrothermal methods as reported in the literatures [20,21]. The presence of terraced surfaces is probably due to the occurrence of 90° domain wall of tetragonal phase as observed in pure $BaTiO_3$ ceramic [21].

3.2 XRD profiles at room temperature

To confirm the perovskite structure of BCZT, the BCZT powder calcined at 1250°C for 3 h and BCZT ceramic sintered at 1400°C for 3 h were analyzed by XRD. The room-temperature XRD profiles are presented in Figure 2 and it was found that both BCZT powder and ceramic showed pure perovskite structure (PDF-00-063-0614)

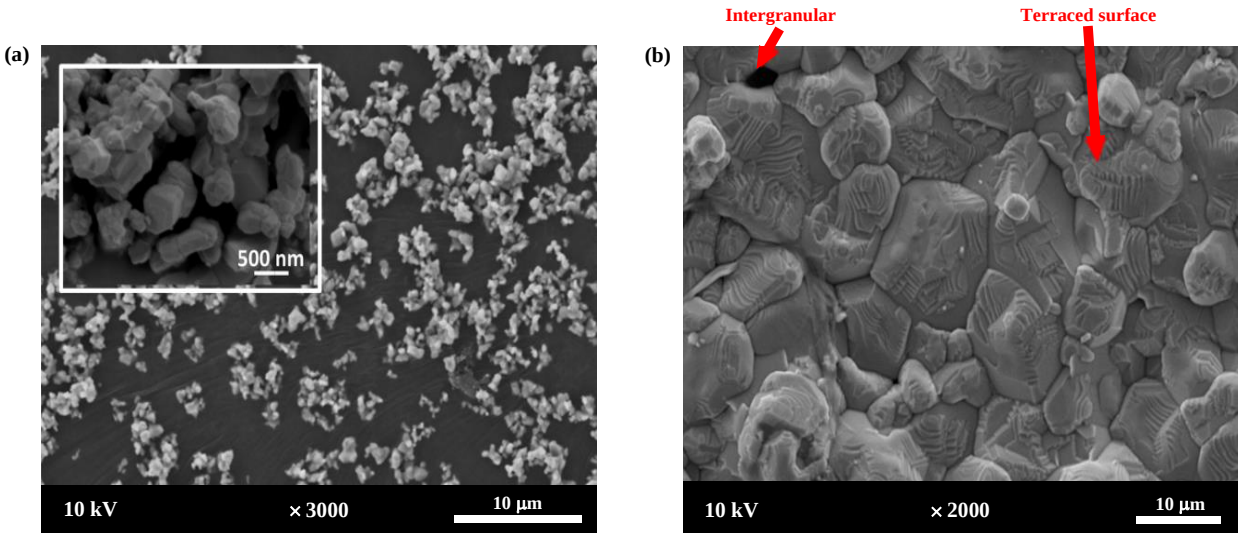

Figure 1. The SEM micrographs of (a) BCZT powder calcined at 1250°C for 3 h and (b) the surface microstructure of BCZT ceramic sintered at 1400°C for 3 h.

without any trace of secondary phases as observed in some literatures near pseudo-cubic $(110)_p$ reflection [11,22]. This indicates clearly that the additions of Ca^{2+} into A-site (or Ba^{2+}-site of pure $BaTiO_3$) and Zr^{4+} into B-site (or Ti^{4+}-site of pure $BaTiO_3$) can be diffused and stabilized in the perovskite structure [22]. Moreover, the enlargement of pseudo-cubic $(200)_p$ reflection for BCZT powder and ceramic is shown in Figure 2(b). It is apparent that peak overlapping can be seen in the enlargement of $(200)_p$ reflection in both powder and ceramic which suggested that the occurrence of mixed phase was observed at room temperature. In addition, the enhancements of sharpness and clear splitting of $(200)_p$ reflection were found in the ceramic sample, indicating the improvement of crystallization from high sintering temperature [15].

Interestingly, although Wang [14] reported that the shifting of $(200)_p$ reflection to lower 2θ was observed in the BCZT ceramic in comparison with the BCZT powder due to the occurrence of the residual stress in the ceramic, this work found the contradict result; the $(200)_p$ reflection of the BCZT ceramic shifts to higher 2θ instead. This implies that the shifting of $(200)_p$ reflection observed in the ceramic sample might not be related to the residual stress but it is possibly due to the enhancement of Ca^{2+} substitution into Ba^{2+} site as using higher temperature for sintering, leading to the shrinkage of unit cell since the ionic radius of Ca^{2+} (1.34 Å) is smaller than Ba^{2+} (1.61 Å) [22].

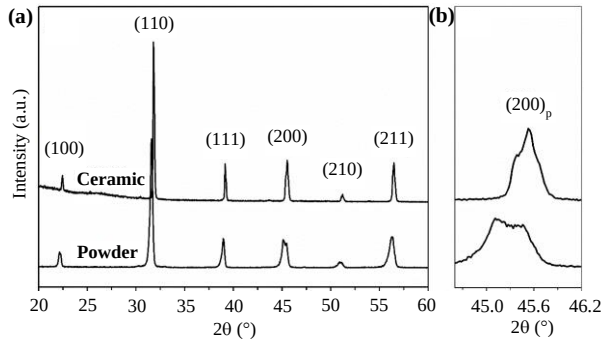

Figure 2. Room-temperature XRD patterns of BCZT powder calcined at 1250°C for 3 h and BCZT ceramic sintered at 1400°C for 3 h in 2θ range of (a) 20° to 60° with (b) the enlargement of $(200)_p$ reflection, showing perovskite structure with $(200)_p$ overlapping peak.

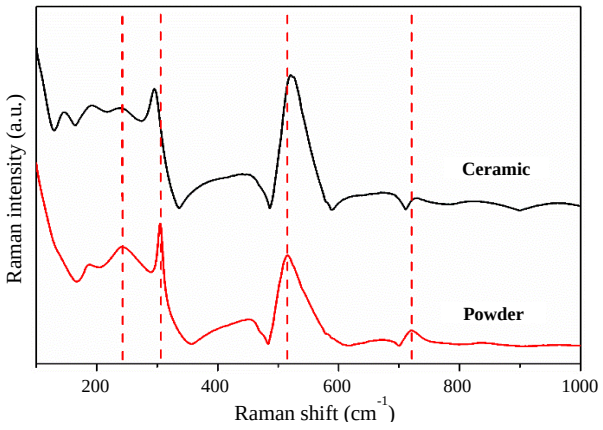

Figure 3. Raman spectra at room temperature for BCZT powder and BCZT ceramic showing the shift at 242, 304, 516 and 720 cm^{-1}, indicated by dash lines.

3.3 Raman spectra

Although the chemical composition of the BCZT powder is similar to the BCZT ceramic in this work, a slight difference was observed in their crystal structure, as discussed earlier in section 0. To clarify this point, Raman spectroscopy was employed to support the XRD result. Figure 3 shows Raman spectra measured at room temperature for the BCZT powder calcined at 1250°C for 3 h and the BCZT ceramic sintered at 1400°C for 3 h. The broad peak observed at 100 cm^{-1} to 300 cm^{-1} is attributed to phonon vibration of Ti-O bonds, while the peaks at 516 cm^{-1} and 720 cm^{-1} are related to Ba-O bonds [23]. It was found that a gradual shift of Raman spectra between the BCZT powder and ceramic was observed; peaks at 242 cm^{-1} and 304 cm^{-1} slightly shifted to lower wavenumber whereas peaks at 516 cm^{-1} and 720 cm^{-1} shifted to higher wavenumber, as seen in Figure 3. This can be explained by the fact that a trace of secondary phase, which commonly are $CaTiO_3$, was possibly found in the BCZT powder but it may not be detected by XRD [18,22]. Therefore, when higher temperature used for sintering the BCZT ceramic, the dissolution of $CaTiO_3$ occurred, leading to the increase of Ca^{2+} substitution into Ba^{2+} site which consequently led to the occurrence of peak shifting. This result was also consistent with the Raman study of $(Ba_{1-x}Ca_x)TiO_3$ ceramic (where x=0.005 and 0.20) investigated by Chang *et al*. [24].

3.4 Temperature-dependent dielectric properties

The dielectric permittivity and loss tangent as a function of temperature between 30°C and 150°C for BCZT ceramic were studied and measured at 1 kHz to 100 kHz (See Figure 4). The diffuse phase transition was observed in the temperature-dependent dielectric permittivity curve, as seen in Figure 4(a). The maximum dielectric permittivity occurred at temperature (T_m) about 92°C, which related to phase transition from ferroelectric to paraelectric phase. Moreover, as frequency increases from 1 kHz to 100 kHz, the maximum of dielectric permittivity at T_m slightly decreases from 6897 to 6635, while T_m gradually shifts from 91.6°C to 91.8°C. The shifting of T_m to higher temperature when the frequency increased indicated the occurrence of relaxor behavior in BCZT ceramic [15]. Note that further analysis in the paraelectric region ($T > T_m$) from Figure 4(a) according to the modified Curie-Weiss law will be determined and shown in Figure 7.

However, there are two peaks that observed in the temperature-dependent loss tangent; at ~39°C and at ~82°C, as seen in Figure 4(b). According to the revised phase diagram of (1-x)BZT-(x)BCT reported by Keeble recently, for x=0.5 or the BCZT composition in this work, the rhombohedral phase should be observed at low temperature (below -13°C) and followed by orthorhombic (from -13°C to 27°C), tetragonal (from 27°C to 93°C) and cubic above 93°C) upon heating [7]. Hence, it can be assumed that the observed peak at near room temperature is associated with phase transition from orthorhombic to tetragonal, while the second peak at high temperature is attributed to phase transformation from tetragonal to cubic. The coexistence of ortho-rhombic and tetragonal at room temperature for the BCZT ceramic and powder will be confirmed by Rietveld refinement as follows.

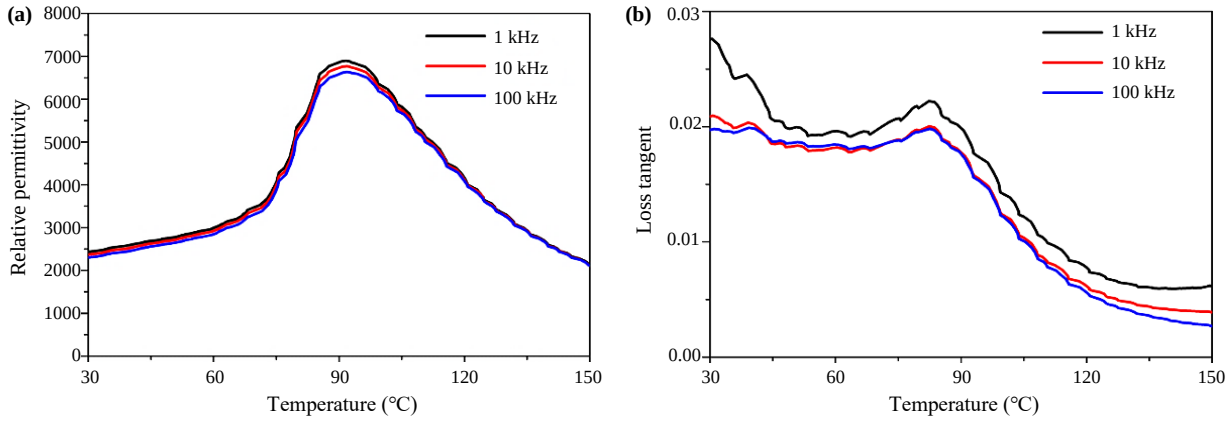

Figure 4. (a) Relative permittivity and (b) Loss tangent as a function of temperature between 30°C and 150°C showing the occurrence of phase transition at room temperature and 92°C, approximately.

3.5 Identification of phase stability at room temperature

Rietveld refinement is a method that developed to analyze X-ray powder diffraction profiles with minimizing issues from the overlapping peak [25]. As a result, it was employed in this work to determine the phase coexistence and the crystallographic information by fitting the observed data (or Obs) with the structure models from the crystallographic information file (CIF file) to obtain the calculated data (or Calc) and the difference between Obs and Calc curves (or diff) [26]. In this work, the crystallographic information files (CIF files) of orthorhombic and tetragonal structures were obtained from crystallography open database (COD) [27]. Note that the CIF files with COD ID-9014492 and COD ID1525437 were used for orthorhombic (Amm2) and tetragonal (P4mm) models, respectively. Figure 5 illustrates the Rietveld refinement for XRD patterns of BCZT powder and ceramic with the coexisting phases of orthorhombic (Amm2) and tetragonal (P4mm), as discussed previously from the temperature-dependent dielectric properties along with the latest phase diagram of (1-x)BZT-(x)BCT. It can be seen that the best-fit refinements for the BCZT powder and ceramic are orthorhombic and tetragonal mixed phase, since the lowest weighted-profile reliability factor (R_{wp}) and Goodness of fit (χ^2) were obtained. The summary of phase fractions, lattice parameters, cell volumes, and refinement parameters for the BCZT powder and ceramic, obtained by Rietveld refinement, is presented in Table 1.

Table 1. Summary of phase fractions, lattice parameters, cell volumes, and refinement parameters for $Ba_{0.85}Ca_{0.15}Ti_{0.9}Zr_{0.1}O_3$ powder and ceramic obtained by Rietveld refinement.

$Ba_{0.85}Ca_{0.15}Ti_{0.9}Zr_{0.1}O_3$ (BCZT)	**Powder**	**Ceramic**
Phase fraction (%)		
Orthorhombic	65.86	40.64
Tetragonal	34.14	59.36
Lattice parameters (Å)		
Orthorhombic		
a	3.99217	4.00002
b	5.66119	5.66822
c	5.70648	5.67528
Tetragonal		
a	3.98903	3.99634
c	4.01216	4.01556
Cell volume (Å^3)		
Orthorhombic	128.969	128.676
Tetragonal	63.843	64.131
Refinement parameters		
R_{wp} (%)	14.282	10.634
Goodness of fit (χ^2)	1.74	1.49

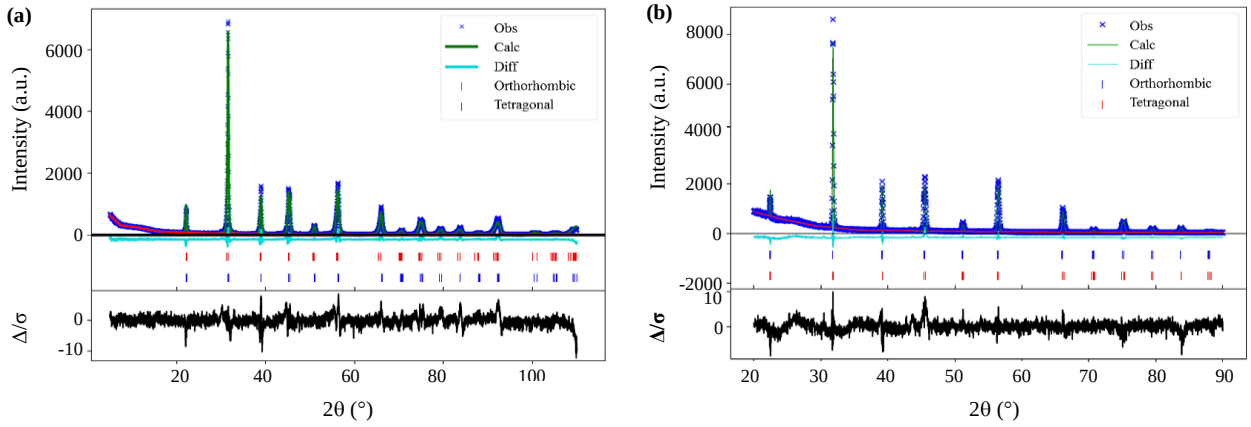

Figure 5. The observed, calculated and difference curves obtained by Rietveld refinement for (a) BCZT powder and (b) BCZT ceramic, showing the best fit with the coexistence of orthorhombic and tetragonal.

In addition, the powder and ceramic samples appear the different phase fractions between O and T. The BCZT powder shows higher O-phase fraction with lower amount of T-phase compared with the BCZT ceramic. This is possibly due to the increase of Ca^{2+} substitution into Ba^{2+} in the ceramic sample, as discussed earlier in section 3.2 and 3.3. Since Keeble [7] mentioned that the addition of Ca^{2+} and Zr^{4+} into $BaTiO_3$ structure can impact on the stabilization of orthorhombic and tetragonal phase, different amount of Ca^{2+} and Zr^{4+} substitutions in the crystal structure can cause the presence of different phase fractions of O and T coexisting phases in the BCZT powder and ceramic.

3.6 Frequency-dependent dielectric properties

The frequency dependence of dielectric permittivity (ε_r) and loss tangent ($\tan\delta$) between 10 Hz to 1 MHz were measured at room temperature and are shown in Figure 6. The maximum ε_r of 2761 was observed at the lowest frequency of 10 Hz. As frequency increased to 1 MHz, the ε_r slightly decreased to 2252 because the response of polarization in the sample gradually dropped [28]. Moreover, the drop of ε_r can also impact on the decrease of piezoelectric voltage coefficient (g) as frequency increases.[4] In term of $\tan\delta$ which related to the domain-wall motion as described by Hardlt [29], it was observed that the decrease of $\tan\delta$ from 0.142 to 0.023 occurred when the frequency increases from 10 Hz to 1 MHz. This evidence demonstrated that lower domain-wall motion was observed as frequency increased which corresponded to the result of frequency-dependent ε_r as well. In comparison to the literature, at frequency of 50 Hz, Buatip observed the maximum room-temperature ε_r of 2844 with $\tan\delta$ of 0.092 for the BCZT ceramic sintered at 1300°C for 4 h, while this work observed little lower ε_r of 2616 and $\tan\delta$ of 0.087 [28].

Further investigation on the relaxor behaviour using the modified Curie-Weiss law to determine the degree of diffuse transition (γ) in paraelectric region ($T > T_m$) at different frequency is shown in Figure 7. Basically, γ of the ideal normal ferroelectric is 1, whereas the ideal relaxor ferroelectric has γ of 2. The equation of the modified Curie-Weiss law is illustrated as follows [30].

$$\frac{1}{\varepsilon_r} - \frac{1}{\varepsilon_m} = \frac{(T - T_m)^\gamma}{C} \quad (1)$$

Note that ε_m is maximum dielectric permittivity and C is Curie-Weiss constant. It was observed that γ of 1.64 was found at the frequency of 1 kHz and slightly increased to 1.68 as frequency increased to 100 kHz, indicating the occurrence of relaxor behavior as mentioned in section 0. This implies that the frequency can impact on the increase of micro-polar cluster, leading to more disorder and higher γ observed in this work [30]. However, there are not only the frequency that can influence on γ, but it is also the grain size. It was found that, as grain size of the BCZT ceramic increased, γ decreased due to the occurrence of long-range ferroelectric interaction and domain thickening, as reported by Wang *et al.* [15].

3.7 Field-dependent ferroelectric P-E loop

The extrinsic contribution of piezoelectric response was determined by the measurement of polarization-electric field (P-E) hysteresis loop in order to understand the evolution of domain switching under the application of electric field, as presented in Figure 8(a). The result shows that, as electric field increases from 5 $kV{\cdot}cm^{-1}$ to 40 $kV{\cdot}cm^{-1}$, the saturated polarization (P_{sat}) increases from 1.74 $\mu C{\cdot}cm^{-2}$ to 13.31 $\mu C{\cdot}cm^{-2}$ and the remnant polarization (P_r) gradually rises from 0.60 $\mu C{\cdot}cm^{-2}$ to 7.43 $\mu C{\cdot}cm^{-2}$, while the coercive field (E_c) is found in a range of 1.48 $kV{\cdot}cm^{-1}$ to 9.07 $kV{\cdot}cm^{-1}$. This is because the application of electric field causes the occurrence of polarization switching and domain growth [31]. Also, at domain-switching field or the E_c in P-E loop, a sudden change of surface charge was observed in the sample, leading to a sharp rise of current density (J) [32]. Figure 8(b) shows changes of current density as a function of electric field of ±40 $kV{\cdot}cm^{-1}$. The abrupt changes were observed at E ~ ±10 $kV{\cdot}cm^{-1}$ in the J-E loop which corresponded to the E_C found in the P-E loop.

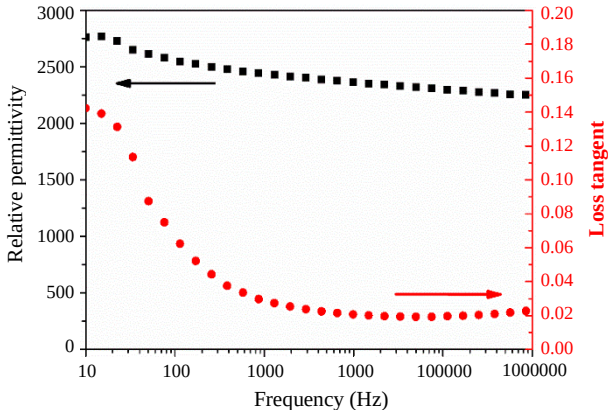

Figure 6. Relative permittivity and loss tangent as a function of frequency from 10 Hz to 1 MHz.

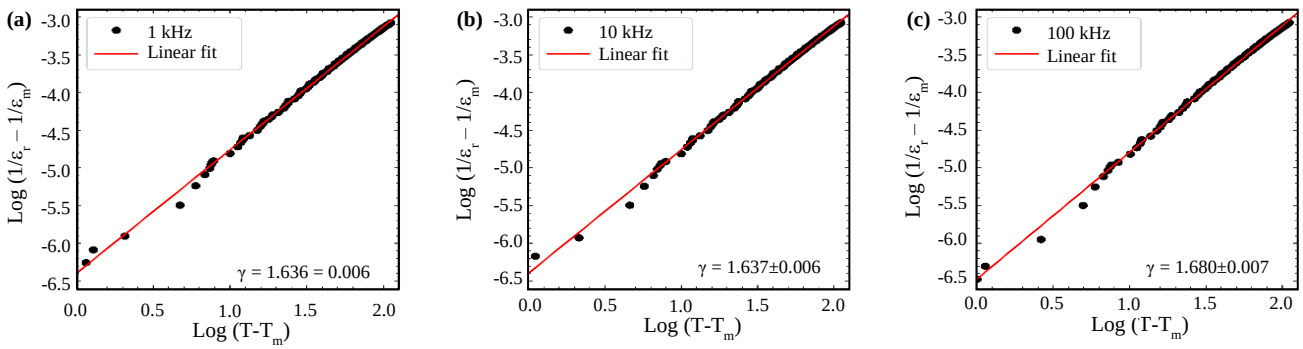

Figure 7. Plot of modified Curie-Weiss law at (a) 1 kHz, (b) 10 kHz, and (c) 100 kHz showing the degree of diffuseness (γ) as a function of frequency.

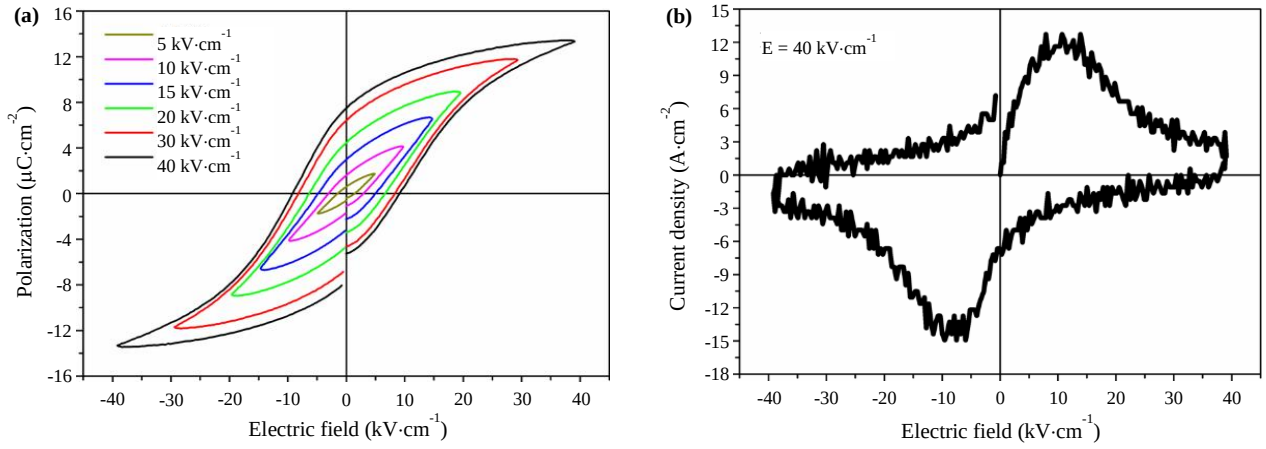

Figure 8. (a) P-E hysteresis loop as a function of electric field and (b) J-E loop of BCZT ceramic measured at room temperature.

4. Conclusions

This work investigated on the phase formation at room temperature of $Ba_{0.85}Ca_{0.15}Ti_{0.9}Zr_{0.1}O_3$ piezoceramic and its functional properties as a function of temperature, frequency and electric field. The room-temperature XRD profiles of the BCZT powder and ceramic showed the overlapping peaks which implies that the mixed phases observed. The temperature-dependent dielectric properties and the latest phase diagram of (1-x)BZT-(x)BCT where x=0.5 suggested that the occurrence of mixed phases at room temperature is the orthorhombic-tetragonal (O-T) coexisting phases. The Rietveld refinement confirmed the coexistence of O-T phases which associated to the intrinsic contribution of piezoelectric response in the BCZT piezoceramics. In addition, this work found that the enhancement of Ca^{2+} substitution into Ba^{2+} site in BCZT ceramic caused the shrinkage of unit cell, leading to the shift of XRD profile as well as Raman spectra. Moreover, it was observed that the functional properties can be influenced by the application of frequency and electric field. These results indicate the impact of frequency and electric field on the domain-wall motion and micro-polar cluster which attributed to the extrinsic contribution of piezoelectric response in the BCZT piezoceramic. Further investigation of the high-resolution synchrotron x-ray powder diffraction (SXPD) profiles as a function of temperature would also help to confirm the coexisting phases at room temperature for the BCZT lead-free piezoceramic.

Acknowledgements

The authors gratefully acknowledge the financial support provided by Faculty of Science and Technology, Thammasat University, Contract No. Sci GR39/2563. Additionally, we thank to Prof. Dr. Naratip Vittayakorn, Advanced Materials Research Unit, Department of Chemistry, Faculty of Science, King Mongkut's Institute of Technology Ladkrabang, Thailand for supporting us on electrical measurements.

References

[1] G.H. Haertling, "Ferroelectric Ceramics: History and Technology," Journal American Ceramic Society, vol. 82, pp. 797-818, 1999.

[2] J. Rödel, and J.-F. Li, "Lead-free piezoceramics: Status and perspectives," *MRS Bulletin*, vol. 43, no. 8, pp. 576-580, 2018.

[3] C-H. Hong, H-P Kim, B-Y. Choi, H-S. Han, J.S. Son, C.W. Ahn, and W. Jo, "Lead-free piezoceramics – Where to move on?," *Journal of Materiomics*, vol. 2, no. 1, pp. 1-24, 2016.

[4] J. Rödel, K.G. Webber, R. Dittmer, W. Jo, M. Kimura, and D. Damjanovic, "Transferring lead-free piezoelectric ceramics into application," *Journal of the European Ceramic Society*, vol. 35, no. 6, pp. 1659-1681, 2015.

[5] W. Liu, and X. Ren, "Large piezoelectric effect in Pb-free ceramics," *Physical Review Letters*, vol. 103, no. 25, pp. 257602, 2009.

[6] M. Acosta, N. Novak, V. Rojas, S. Patel, R. Vaish, J. Koruza, G.A. Rossetti Jr, and J. Rödel "$BaTiO_3$-based piezoelectrics: Fundamentals, current status, and perspectives," *Applied Physics Reviews*, vol. 4, no. 4, pp. 041305, 2017.

[7] D.S. Keeble, F. Benabdallah, P.A. Thomas, M. Maglione, and J. Kreisel, "Revised structural phase diagram of $(Ba_{0.7}Ca_{0.3}TiO_3)$-$(BaZr_{0.2}Ti_{0.8}O_3)$," *Applied Physics Letters*, vol. 102, no. 9, pp. 092903, 2013.

[8] A. Bjørnetun Haugen, J.S. Forrester, D. Damjanovic, B. Li, K.J. Bowman, and J.L. Jones, "Structure and phase transitions in $0.5(Ba_{0.7}Ca_{0.3}TiO_3)$-$0.5(BaZr_{0.2}Ti_{0.8}O_3)$ from −100°C to 150°C," *Journal of Applied Physics*, vol. 113, no. 1, pp. 014103, 2013.

[9] D. Tuan, V. Thanh Tung, L. Tu, and T. Chuong, "Synthesis and Investigation of the Physical Properties of Lead-Free BCZT Ceramics," in *Perovskite and Piezoelectric Materials*, 2019.

[10] X. Ji, C. Wang, S. Li, S. Zhang, R. Tu, Q. Shen, J. Shi, and L. Zhang, "Structural and electrical properties of BCZT ceramics synthesized by sol–gel process," *Journal of Materials Science: Materials in Electronics*, vol. 29, no. 9, pp. 7592-7599, 2018.

[11] P. Mishra, Sonia, and P. Kumar, "Effect of sintering temperature on dielectric, piezoelectric and ferroelectric properties of BZT–BCT 50/50 ceramics," *Journal of Alloys and Compounds*, vol. 545, pp. 210-215, 2012.

[12] Z. Hanani, D. Mezzane, M'barek Amjoud, Y. Gagou, K. Hoummada, C. Perrin, A.G. Razumnaya, Z. Kutnjak, A. Bouzina, M. El Marssi, M. Gouné, and B. Rožič, "Structural, dielectric, and ferroelectric properties of lead-free BCZT ceramics elaborated by low-temperature hydrothermal processing," *Journal*

of Materials Science: Materials in Electronics, vol. 31, no. 13, pp. 10096-10104, 2020.

[13] M.B. Abdessalem, S. Aydi, A. Aydi, N. Abdelmoula, Z. Sassi, and H. Khemakhem, "Polymorphic phase transition and morphotropic phase boundary in $Ba_{1-x}Ca_xTi_{1-y}Zr_yO_3$ ceramics," *Applied Physics A*, vol. 123, no. 9, pp. 583, 2017.

[14] W. Wang, W. L. Li, D. Xu, W.P. Cao, Y.F. Hou, and W.D. Fei, "Phase transitions in (1-x)$BaZr_{0.2}Ti_{0.8}O_3$-x$Ba_{0.7}Ca_{0.3}TiO_3$ powders and ceramic pellets," *Ceramics International*, vol. 40, no. 3, pp. 3933-3937, 2014.

[15] X. Wang, B.H. Zhang, Y.Y. Li, Y.C. Shi, L.Y. Sun, G. Feng, C.L. Li, Y.F. Liang, Y.P. Zheng, S.Y. Shang, J. Shang, and Y. Hu, "Structure, dielectric, and ferroelectric properties of $Ba_{0.85}Ca_{0.15}Zr_{0.1}Ti_{0.9}O_3$ ceramics sintered at various temperatures," *Journal of Materials Science-Materials in Electronics*, vol. 31, no. 6, pp. 4732-4742, Mar 2020.

[16] D.A. Ochoa Guerrero, G. Esteves, T. Iamsasri, F. Rubio-Marcos, J.F. Fernández Lozano, J.E. Garcia, and J.L. Jones, "Extensive domain wall contribution to strain in a (K,Na) NbO_3-based lead-free piezoceramics quantified from high energy X-ray diffraction," *Journal of the European Ceramic Society*, vol. 36, no. 10, pp. 2489-2494, 2016.

[17] B.H. Toby, and R.B. Von Dreele, "GSAS-II: the genesis of a modern open-source all purpose crystallography software package," *Journal of Applied Crystallography*, vol. 46, no. 2, pp. 544-549, 2013.

[18] P. Wang, Y. Li, and Y. Lu, "Enhanced piezoelectric properties of $(Ba_{0.85}Ca_{0.15})(Ti_{0.9}Zr_{0.1})O_3$ lead-free ceramics by optimizing calcination and sintering temperature," *Journal of the European Ceramic Society*, vol. 31, no. 11, pp. 2005-2012, 2011.

[19] W. Ji, B. Fang, X. Lu, S. Zhang, N. Yuan, and J. Ding, "Tailoring structure and performance of BCZT ceramics prepared via hydrothermal method," *Physica B: Condensed Matter*, vol. 567, pp. 65-78, 2019.

[20] G. Herrera-Pérez, I. Castillo-Sandoval, O. Solís-Canto, G. Tapia-Padilla, A. Reyes-Rojas, and L. E. Fuentes-Cobas, "Local piezo-response for lead-free $Ba_{0.9}Ca_{0.1}Ti_{0.9}Zr_{0.1}O_3$ electro-ceramic by switching spectroscopy," *Materials Research*, vol. 21, no. 2, 2018.

[21] M. Gao, W. Ge, X. Li, H. Yuan, C. Liu, H. Zhao, Y. Ma, and Y. Chang, "Enhanced dielectric and energy storage properties in Fe-Doped BCZT ferroelectric ceramics," *physica status solidi (a)*, vol. 217, no. 16, pp. 2000253, 2020.

[22] W. Li, Z. Xu, R. Chu, P. Fu, and G. Zang, "Structural and dielectric properties in the $(Ba_{1-x}Ca_x)(Ti_{0.95}Zr_{0.05})O_3$ ceramics," *Current Applied Physics*, vol. 12, no. 3, pp. 748-751, 2012.

[23] R. Hayati, M. A. Bahrevar, T. Ebadzadeh, V. Rojas, N. Novak, and J. Koruza, "Effects of Bi_2O_3 additive on sintering process and dielectric, ferroelectric, and piezoelectric properties of $(Ba_{0.85}Ca_{0.15})(Zr_{0.1}Ti_{0.9})O_3$ lead-free piezoceramics," *Journal of the European Ceramic Society*, vol. 36, no. 14, pp. 3391-3400, 2016.

[24] M.C. Chang, and S. -C. Yu, "Raman study for $(Ba_{1-x}Ca_x)TiO_3$ and $Ba(Ti_{1-y}Ca_y)O_3$ crystalline ceramics," *Journal of Materials Science Letters*, vol. 19, no. 15, pp. 1323-1325, 2000.

[25] H.M. Rietveld, "A Profile Refinement Method for Nuclear and Magnetic Structures," *Journal of Applied Crystallography*, vol. 2, pp. 65-71, 1969.

[26] B.H. Toby, "R factors in Rietveld analysis: How good is good enough?," *Powder diffraction*, vol. 21, no. 1, pp. 67-70, 2006.

[27] S. Grazulis, D. Chateigner, R.T. Downs, A.F.T. Yokochi, M. Quiros, L. Lutterotti, E. Manakova, J. Butkus, P. Moeck, and A. Le Bail, "Crystallography Open Database - an open-access collection of crystal structures," *Journal Applied Crystallography*, vol. 42, no. Part 4, pp. 726-729, 2009.

[28] N. Buatip, N. Promsawat, N. Pisitpipathsin, O. Namsar, P. Pawasri, K. Ounsung, K. Phabsimma, S.T. Rattananchan, P. Janphuang, and S. Projprapai, "Investigation on electrical properties of BCZT ferroelectric ceramics prepared at various sintering conditions," *Integrated Ferroelectrics*, vol. 187, no. 1, pp. 45-52, 2018.

[29] K.H. Hardtl, "Electrical and Mechanical Losses in Ferroelectric Ceramics," *Ceramics International*, vol. 8, pp. 121-127, 1982.

[30] Z. Raddaoui, S. El Kossi, J. Dhahri, N. Abdelmoula, and K. Taibi, "Study of diffuse phase transition and relaxor ferroelectric behavior of $Ba_{0.97}Bi_{0.02}Ti_{0.9}Zr_{0.05}Nb_{0.04}O_3$ ceramic," *RSC Advances*, vol. 9, no. 5, pp. 2412-2425, 2019.

[31] P.M. Dragan Damjanovic, and Nava Setter, "Ferroelectric Sensors," *IEEE SENSORS JOURNAL*, vol. 1, pp. 191-206, 2001.

[32] X. Chao, Z. Wang, Y. Tian, Y. Zhou, and Z. Yang, "$Ba(Cu_{0.5}W_{0.5})O_3$-induced sinterability, electrical and mechanical properties of $(Ba_{0.85}Ca_{0.15}Ti_{0.90}Zr_{0.10})O_3$ ceramics sintered at low temperature," *Materials Research Bulletin*, vol. 66, pp. 16-25, 2015.